

Phonon coupling to excitations of free and localized electrons in *n*-type ZnSe

D. J. Olego, T. Marshall, J. Gaines, and K. Shahzad

Philips Laboratories, North American Philips Corporation, Briarcliff Manor, New York 10510

(Received 25 June 1990)

The coupling mechanisms between longitudinal-optical phonons and electronic excitations in *n*-type ZnSe layers were investigated with Raman spectroscopy in conjunction with transport measurements. The layers were grown by molecular-beam epitaxy and were intentionally doped below the Mott criterion for the insulator-metal transition. The nature of the electron-phonon interaction is determined by the degree of electron localization, which was effectively changed by temperature and donor concentration. The longitudinal-optical phonons couple to plasmons when electrons are thermally excited into the conduction band and to a continuum of electronic excitations when electrons are localized in an impurity band or at donor sites. In both cases unbound phonons are observed. From the renormalized phonon frequencies at high temperature, values of free-electron concentration as a function of temperature were established. They are in excellent agreement with Hall-effect determinations. At low temperatures the phonon Raman profiles are asymmetric and show Fano-type line shapes. The electronic continuum responsible for the phonon self-energies at low temperature was identified as Raman scattering by bound electrons.

I. INTRODUCTION

The interaction between electrons and optical phonons in doped semiconductors has been extensively investigated in recent years with inelastic light scattering. Most of these investigations were carried out in group IV or III-V semiconducting materials. In the elemental semiconductors, the phonons couple to interband and intraband excitations of the carriers through the deformation-potential mechanism. Striking quantum-interference effects with associated changes in phonon self-energies result from this coupling in *p*-type Si and Ge and *n*-type Si.^{1,2} In the polar materials, such as GaAs, the nature of the coupling depends markedly on the transverse or longitudinal character of the phonons. For example, the macroscopic electric field of the longitudinal phonons interacts very strongly with the charge-density fluctuation of the free carriers giving rise to the so-called coupled plasmon-phonon modes.^{1,2} The renormalization of the phonon frequencies due to this interaction is, in most instances, much larger than those yielded by the self-energy contributions of the deformation potential.

In contrast to the case of group IV and III-V materials far less experimental work on this subject has been reported in doped II-VI semiconductors, particularly in the "wide-band-gap" system represented by ZnSe, ZnS, and ZnTe. The lack of experimental reports stems in part from the difficulties encountered in producing samples with reproducible parameters by conventional bulk-growth techniques. Recent developments in advanced deposition techniques for thin films now allow the growth of II-VI epitaxial layers with high structural quality and reproducible optoelectronic properties including doping.³ This, in turn, has renewed the interest in the characterization and fundamental properties of these materials.

We report here on the mechanisms of the electron-phonon interaction in *n*-type ZnSe layers, which were in-

tentionally doped with shallow donors in concentrations below the Mott criterion for the metal-insulator transition. The coupling mechanism between the longitudinal-optical phonons and the electronic excitations were established by performing Raman-scattering experiments and by correlating them with measurements of transport properties carried out in the same samples. We have monitored the Raman frequencies and line shapes for different degrees of electron localization and we will show that the longitudinal-optical phonons of ZnSe can either form a coupled system with the plasmons or display self-energy effects typical of discrete-continuum interactions. Temperature is a very effective way to control localization of electron wave functions in ZnSe because the ionization energy E_D of donors ranges between 25 and 28 meV.⁴ This means that at room temperature most of the donor atoms have contributed their electrons to delocalized conduction-band states.⁵ Conversely, when $k_B T \ll E_D$ (k_B is the Boltzmann constant) strong localization of the electrons is expected either at the donor sites or, as the concentration approaches the metal-insulator transition, in an impurity band.⁶

The organization of the paper is as follows. Section II gives an account of the sample growth and experimental conditions of the optical and transport measurements. Section III summarizes the relevant transport properties for the interpretation of the Raman results, which are presented and discussed in Sec. IV. Concluding remarks are given in Sec. V.

II. EXPERIMENTAL

The ZnSe layers were grown by molecular-beam epitaxy (MBE) on (001) surfaces of GaAs wafers. High-purity elemental sources of Zn and Se were used to generate the molecular beams for the ZnSe growth and doping was achieved *in situ* with a source of In. Before the

ZnSe deposition, the GaAs surfaces were chemically cleaned and the native oxide was desorbed following standard MBE procedures.⁷ Typical substrate temperatures for growth were around 300°C and growth rates were of the order of 1 μm an hour. The flux stoichiometry ratio Zn to Se was 1:2 and the layer thicknesses range between 3 and 4 μm . The donor concentrations were determined from the Hall effect and capacitance versus voltage measurements. The Hall-effect measurements were carried out in the van der Pauw geometry with layers grown on semi-insulating substrates. The metal contacts were provided by In deposited on the sample surfaces after growth. The capacitance versus voltage characterization was done in structures grown on *n*-type GaAs substrates with Au dots for contacts on the ZnSe surface and In on the back surface of the substrate.

The Raman experiments were conducted in back-scattering geometry with the exciting and scattered light propagating along the [001] and the [00 $\bar{1}$] directions, respectively. The polarization of the incoming and scattering photons was along [110]. This scattering geometry is described by the standard notation $z(x+y, x+y)\bar{z}$.^{1,2} Most of the Raman spectra were excited with the 488.0 nm (2.54 eV) visible line of an Ar⁺-ion laser operating in a continuous wave mode. The energy of such laser photons is smaller than the fundamental band edge of ZnSe, which lies between 2.63 and 2.82 eV going from room temperature down to 4 K.⁸ The Raman-scattered light is generated in the entire volume of the epitaxial layers and, therefore, it is representative of the doped bulk portion of the ZnSe specimen. Contributions to the total Raman signal from light scattered in depleted space-charge regions at the ZnSe-air or ZnSe-GaAs interfaces are expected to be negligible with the below band-gap excitation.² The Raman-scattered photons were analyzed with a Spex 1404 double monochromator and detected with photon counting electrons. The reproducibility of Raman peak positions was better than $\pm 0.1 \text{ cm}^{-1}$. For the temperature-dependent measurements, the samples were mounted on a copper cold finger of a closed cycle He cryostat. The temperature was tuned between 300 and 12 K with an accuracy better than $\pm 0.2 \text{ K}$.

III. SUMMARY OF TRANSPORT PROPERTIES

The dots in Fig. 1 represent results of Hall-effect measurements as a function of temperature T for a typical *n*-type-doped ZnSe layer. One can see that the values of $(R_H e)^{-1}$, where R_H is the Hall coefficient and e is the electron charge, display a pronounced dip in the neighborhood of 50 K. The presence of this dip and the overall dependence on T correspond to a "two-carrier system" in which impurity band conduction occurs along with transport in the conduction band.⁶ For T above the one corresponding to the dip in $(R_H e)^{-1}$, transport is dominated by free carriers populating delocalized states of the conduction band. On the right-hand side of the minimum in $(R_H e)^{-1}$ for $T < 50 \text{ K}$, conduction proceeds through localized states of an impurity band. These qualitative conclusions can be rigorously obtained by appropriate modeling of the Hall-effect results.⁶ In particu-

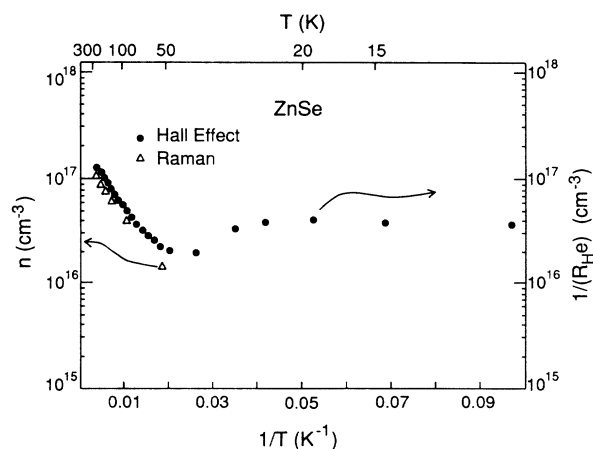


FIG. 1. Hall-effect results as a function of temperature for a typical *n*-type doped ZnSe layer with $1.7 \times 10^{17} \text{ donors cm}^{-3}$ grown by molecular-beam epitaxy. The dip in the inverse of the Hall coefficient R_H at around 50 K establishes the presence of a two-carrier system. Temperatures larger than 50 K activate electrons into conduction-band states. The free-electron concentration $n(T)$ is then given by $(R_H e)^{-1}$. At temperatures below 50 K, conduction in an impurity band dominates. The optically established carrier concentration is plotted for comparison. Good agreement is obtained with the transport determination.

lar, it can be shown that for $T \geq 100 \text{ K}$ the free-carrier concentration $n(T)$ in the conduction band is given by $n(T) = (R_H e)^{-1}$.

The decrease of $n(T)$ with decreasing T from 300 to 100 K is due to the progressive freeze out of the electrons. A model fit to $n(T)$ in the range of T with the standard expressions of semiconductor statistics yields a donor concentration N_D of $1.7 \times 10^{17} \text{ cm}^{-3}$ with a compensation ratio of 0.08 and an activation energy of 14 meV to promote carriers into the delocalized conduction states.⁵ The so-determined N_D is smaller than the predicted donor concentration of $\approx 4 \times 10^{17} \text{ cm}^{-3}$ for the Mott insulator-metal transition in ZnSe.⁶ Therefore, the impurity band comes about from partial overlap of donor wave functions or broadening of donor orbitals by potential fluctuations.

Conductivity and mobility measurements reinforce the interpretation of the Hall-effect data; in particular, the presence of localized carriers at low T . Between 300 and 100 K the functional dependence of the conductivity σ on T takes the form $\ln \sigma \propto -T^{-1}$, which is the expected behavior for free carriers. Below 50 K a dependence of the type $\ln \sigma \propto -T^{-1/4}$ is measured, which identifies the conduction mechanism in the impurity band as variable range hopping.⁶ The mobility as a function of T also shows the transition from one conduction regime to another. Room temperature mobility for the sample of Fig. 1 is $400 \text{ cm}^2/\text{V sec}$, which is a state of the art value for a doped sample in the low $10^{17} \text{ donors cm}^{-3}$ range. With decreasing T the mobility increases steadily and reaches a maximum value of $800 \text{ cm}^2/\text{V sec}$ at $T \approx 100 \text{ K}$. Further cooling of the sample decreases the mobility, but

at a smaller rate than the one expected if free carriers are subject to impurity scattering after phonons have been quenched.⁵ Below 50 K, the mobility settles slowly to a more or less constant value of 40 cm²/V sec. This is much larger than any calculated mobility value for non-degenerate ZnSe with free-carrier concentration determined by semiconductor statistics and impurity scattering as the main scattering process. It is in line with the transport process inferred from the conductivity data for localized electrons.

IV. RAMAN SCATTERING RESULTS AND DISCUSSION

Figure 2 compares first-order Raman spectra of doped and undoped ZnSe layers for selected values of T . These spectra were excited with 488.0-nm laser radiation and arise from scattering by long-wavelength longitudinal-optical (LO) modes, which are allowed by the scattering selection rules for the geometry described in Sec. II.² The undoped layer is semi-insulating and its free-carrier concentration at 300 K is less than 10¹⁴ electrons cm⁻³. The doped layer is the one whose transport properties were described in the preceding section and given in Fig. 1.

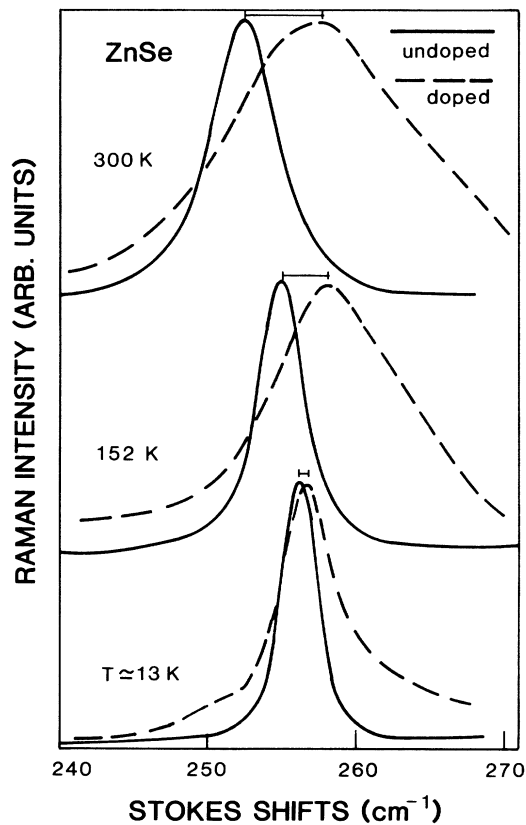


FIG. 2. Raman spectra of longitudinal-optical phonons for doped (1.7×10^{17} donors cm⁻³) and undoped ZnSe layers excited with 488.0-nm laser radiation. The scattering geometry is given by $z(x+y, x+y)\bar{z}$ and this notation is described in Sec. II. The peaks for the doped layer are shifted to higher frequencies at all temperatures. The lineshape for the doped sample at 13 K displays asymmetrical broadening.

The striking feature of the data in Fig. 2 is the shift to higher frequencies of the spectra corresponding to the doped layer when compared with those of the reference sample. In addition, these spectra are substantially broader. At the lowest T , they display a pronounced asymmetry towards the high-energy side.

The measured peak positions for the doped and control samples are plotted against T in Fig. 3. The LO frequencies of the undoped sample, which we will label Ω_{LO} in this discussion, show a clear softening with increasing T . This effect, which has been seen already in ZnSe and other semiconductors, arises from anharmonic contributions in the phonon-phonon interaction.⁹⁻¹¹ In the plot of the frequencies of the doped layer, referred to as $\Omega_{LO}^{\text{doped}}$, we can distinguish a kink at around 60 K. Contrary to the well-established softening of Ω_{LO} with T , $\Omega_{LO}^{\text{doped}}$ increases monotonically between 60 and 300 K. Below 60 K, it does not change with T within the experimental uncertainty although it remains slightly higher than Ω_{LO} . We note that the kink in the temperature dependence of $\Omega_{LO}^{\text{doped}}$ occurs at comparable temperatures as the dip in $(R_{He})^{-1}$ shown in Fig. 1. We will argue that, just like the dip in $(R_{He})^{-1}$ indicates a transition from localization to delocalization in the electron system, the kink in the frequency plot of $\Omega_{LO}^{\text{doped}}$ establishes a transition between two different modes of electron-phonon coupling in the doped layers.

We postulate that above 100 K the upward renormalization of $\Omega_{LO}^{\text{doped}}$ is due to the coupling of the phonons with the charge-density fluctuations of the free carriers, which populate the conduction band with a density $n(T)$. The Raman modes of the doped sample in Fig. 2 for

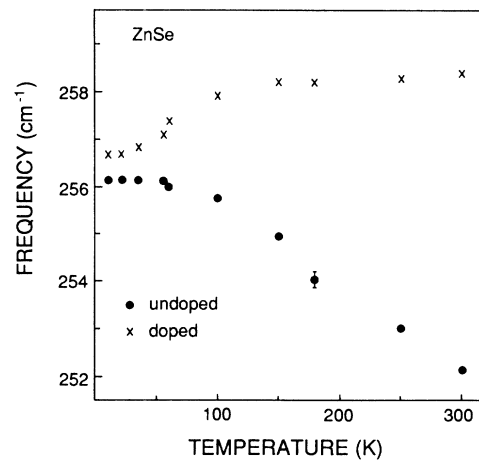


FIG. 3. Peak frequencies of the Raman spectra measured in the previous figure as a function of temperature. The frequencies of the undoped layer are labeled Ω_{LO} in the text. In the case of the doped sample the notation $\Omega_{LO}^{\text{doped}}$ is being used. Notice the kink in the plot of the doped frequencies. It happens at around the same temperature as the dip in $(R_{He})^{-1}$ seen in Fig. 1. Between 13 and 50 K a discrete-continuum interaction renormalizes the doped frequencies. Above 100 K the plasmon-phonon coupling is responsible for their substantial upward shift.

$100 < T < 300$ K are then identified as the phononlike component of the plasmon-phonon coupled modes.^{1,2} Under this assumption, $\Omega_{LO}^{\text{doped}}$ is given by the relationship

$$\Omega_p^2 = \Omega_{LO}^{\text{doped}^2} \frac{\Omega_{LO}^2 - \Omega_{LO}^{\text{doped}^2}}{\Omega_{TO}^2 - \Omega_{LO}^{\text{doped}^2}}, \quad (1)$$

where Ω_{TO} is the temperature-dependent frequency of the transverse-optical (TO) phonons in the undoped sample and Ω_p is the plasma frequency of the charge-density excitations of the free electrons in the doped sample. The plasma frequency is related to the temperature-dependent electron concentration $n(T)$ through the expression

$$\Omega_p^2 = \frac{n(T)e^2}{\epsilon_\infty m^*}, \quad (2)$$

in which ϵ_∞ and m^* are the high-frequency dielectric constant and the conduction-band effective mass, respectively. Therefore, one way to test the validity of the above-stated description is by determining with the help of Eqs. (1) and (2) “optical values” of $n(T)$ and by comparing them with the transport determination. With Ω_{LO} and $\Omega_{LO}^{\text{doped}}$ taken from Fig. 3 for $T > 100$ K, measured values of Ω_{TO} as a function of T (not shown here, but we have established that the Ω_{LO} - Ω_{TO} splitting is 46.5 cm^{-1} and is independent of T), $\epsilon_\infty = 6.1$ and $m^* = 0.16$,⁸ we obtained the values of $n(T)$ represented by the open triangles in Fig. 1.

The optical and transport determinations compare very favorably, thus justifying the assumptions about the phonon-plasmon coupling. Minor quantitative disagreements (less than 10%) are probably the result of not having considered any dependence of m^* on $n(T)$. The overall good agreement in Fig. 1 is also an indication that $\Omega_{LO}^{\text{doped}}$ is not mobility limited for N_D up to low 10^{17} donors cm^{-3} and that wave-vector nonconservation does not play a leading role in the light-scattering process of these doped layers.² The increasing splitting $\Omega_{LO}^{\text{doped}} - \Omega_{LO}$ with T above 100 K in Fig. 3 is a lucid manifestation in the optical properties of the ionization of the donors with the associated population of conduction-band states by electrons. We have also studied samples with lower donor concentrations ($10^{16} < N_D < 10^{17} \text{ cm}^{-3}$). As expected the splittings between the doped and undoped frequencies for a given T decrease with N_D but the general behavior is similar to the one shown in Fig. 3. A successful determination of $n(T)$ with an optical technique in a wide-band-gap semiconductor is relevant from a technological point of view. In many of the intended solid-state devices comprising the wide-band-gap II-VI semiconductors, one finds them as buried layers between materials of even larger forbidden gaps. Direct access to the carriers with conventional transport techniques becomes extremely difficult under such conditions. Also, for certain types of doping (for example, p -type ZnSe and n -type ZnTe) the technology of reliable metal ohmic contacts is lacking and alternative ways to ascertain the presence of carriers and hence the activation of a dopant atom are of furthestmost priority.

To explain the origin of the small shift in $\Omega_{LO}^{\text{doped}}$ for

$T < 50$ K in Fig. 3 we invoke a discrete-continuum type interaction, in which the discrete state of the LO phonon couples to a continuum of excitations of the now localized electrons. Insight into the nature of the electronic excitations producing the continuum was gained by performing Raman experiments with laser energy below but close to the fundamental gap of ZnSe. We present in Fig. 4 Raman results obtained with laser light at 457.9 nm (2.71 eV) which happens to be in near resonance with the low-energy side of a weak and featureless luminescence background below the gap. In addition to the slightly upward shifted LO-phonon line at 256.8 cm^{-1} , a broad band appears in the Raman spectrum. This extra Raman signal was not observed with the 488.0-nm laser excitation of Fig. 2. It corresponds to electronic Raman scattering from transitions between bound donor states. This process, which is depicted in the inset to Fig. 4, provides the electronic continuum that interacts with the photon. The peak riding on the broad band at around 210 cm^{-1} arises from scattering by the TO phonons due probably to some relaxation in the selection rules. The two lower-energy features at around 175 and 197 cm^{-1} can be identified with the $1s$ - $2s$ and $1s$ - $3s$ transitions of the donors.⁴ Scattering to the right-hand side of the TO line spreading all the way up to the LO peak is due to transitions from the $1s$ fundamental state to levels at or

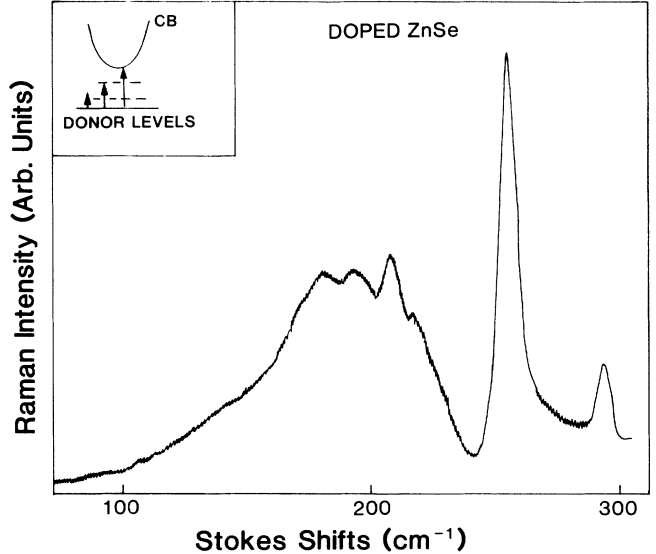


FIG. 4. Raman spectrum of a doped ZnSe layer (1.7×10^{17} donors cm^{-3}) taken at 13 K with laser photons at 457.9 nm in the scattering geometry of Fig. 2. The longitudinal-optical phonon peak at 256.8 cm^{-1} is prominently seen and towards lower frequencies the broad band is resonant electronic Raman scattering by bound electrons. The inset depicts such a process. The asymmetry in the phonon line shape seen in Fig. 2 is also observed here. A weak antiresonance on the low-energy side of the phonon peak can be distinguished. The weaker structure at around 295 cm^{-1} is due to the longitudinal-optical phonon of the GaAs substrate. It is observed because the ZnSe layer is transparent to the incoming laser radiation.

above the ionization threshold of the donors. For an isolated In donor E_D is 28.2 meV (225 cm^{-1}).⁴ The electronic transitions that in isolated donors will be of discrete nature are broadened in the doped samples for the same reasons that the impurity band is formed. It is intriguing that spectroscopical signatures of individual donors are observed though the transport proceeds through an impurity band. The high-energy side of the electronic continuum overlaps with the LO-phonon line and a weak antiresonance is observed just before the LO-peak maximum. The asymmetrical broadening of the phonon line already seen in the data of Fig. 2 is apparent in Fig. 4.

In the framework of the discrete-continuum interaction the renormalization of the phonon frequency in the doped sample $\Omega_{\text{LO}}^{\text{doped}}$ is given by^{1,2}

$$\Omega_{\text{LO}}^{\text{doped}} = \Omega_{\text{LO}} + V^2 R(E), \quad (3)$$

where V is the matrix element for the coupling between the discrete phonon state and the continuum of electronic excitations and $R(E)$ is the Hilbert transform of the density $\rho(E)$ of continuum states. To perform a quantitative comparison between theory and experiment we need a microscopic model for V and $R(E)$ which we lack presently. Renormalization of phonon frequencies due to interactions with bound electron or hole excitations of the type $1s$ - $2s$ have been reported in doped semiconductors.^{1,12-14} A convenient way to observe these interactions is in the phonon replica of photoluminescence either from recombinations of neutral donor and acceptor bound excitons or from the so-called “two-electron” or “two-hole” transitions. In most cases, the phonon energy is less than the $1s$ - $2s$ energy and the result of the interaction is the creation of bound phonons with smaller frequencies in the neighborhood of the impurity. The situation considered here is quite different as the LO phonons remain unbound and their frequencies increase. Another important point is that the electronic continuum is not provided by intraband transitions of free carriers at the zone center because symmetry considerations preclude in such case coupling with zone-center phonons.² The kind of discrete-continuum interaction considered here can lead to the asymmetries measured in the LO line shapes in Figs. 2 and 4 because of quantum-mechanical interference. Indeed, the Fano-Breit-Wigner profile provides a good fit to these asymmetrical line shapes. The dependence of the Fano fitting parameters and behavior of the electronic scattering on laser wavelength and N_D go beyond the scope of the present work and will be dealt with separately.

The interaction with the electrons not only renormalizes the frequency of the phonons but changes their lifetimes as well. The latter effect shows up in broader Raman lines for the doped samples. The breadths at half maximum of the Raman peaks in Fig. 2 corrected for spectrometer resolution and those of samples with smaller N_D are plotted against T in Fig. 5. The correlation between N_D and the symbols used in Fig. 5 is explained in the figure caption. The increase with T of the LO-phonon linewidth Γ_{LO} in the undoped sample is due to anharmonic decay into acoustic phonons.⁹⁻¹¹ In the

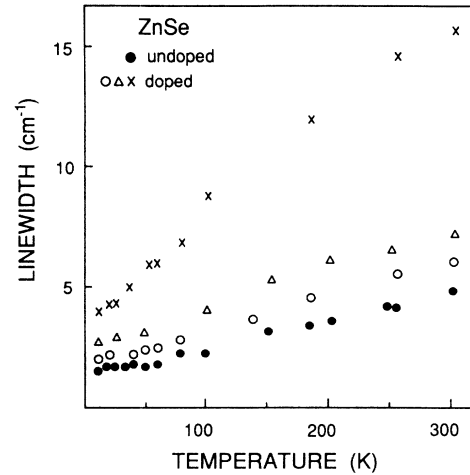


FIG. 5. Linewidths of the Raman peaks of ZnSe layers measured with 488.0-nm laser excitation as a function of temperature. The data have been corrected for instrumental resolution. In the text, the linewidths of the undoped layer are labeled Γ_{LO} and those of the doped samples $\Gamma_{\text{LO}}^{\text{doped}}$. The donor concentration N_D of the doped samples is the following: crosses, $1.7 \times 10^{17} \text{ donors cm}^{-3}$; open triangles, $3.6 \times 10^{16} \text{ donors cm}^{-3}$; and open circles, $2.1 \times 10^{16} \text{ donors cm}^{-3}$, respectively. The broadening $\Gamma_{\text{LO}}^{\text{doped}} - \Gamma_{\text{LO}}$ increases with temperature when electrons populate conduction-band states and remains constant when the electrons are subject to localization.

doped samples the linewidth $\Gamma_{\text{LO}}^{\text{doped}}$ also increases with T and for a given T with N_D . The contribution to $\Gamma_{\text{LO}}^{\text{doped}}$ of the electron-phonon interaction is determined by the broadening $\Gamma_{\text{LO}}^{\text{doped}} - \Gamma_{\text{LO}}$, which excludes the thermal effects. An inspection of the behavior of $\Gamma_{\text{LO}}^{\text{doped}}$ in Fig. 5 also indicates the presence of two regimes depending on the degree of electron localization. When the electrons are localized, $\Gamma_{\text{LO}}^{\text{doped}} - \Gamma_{\text{LO}}$ remains more or less constant with increasing T . On the other hand, when free electrons start to populate the conduction band as evidenced by $\Omega_{\text{LO}}^{\text{doped}}$ and the Hall effect, $\Gamma_{\text{LO}}^{\text{doped}}$ deviates markedly from Γ_{LO} and $\Gamma_{\text{LO}}^{\text{doped}} - \Gamma_{\text{LO}}$ substantially increases. The value of T at which this change in behavior takes place increases with decreasing N_D . In Fig. 5 we observe that it occurs at around 50, 100, and 150 K for N_D 1.7×10^{17} , 3.6×10^{16} , and $2.1 \times 10^{16} \text{ donors cm}^{-3}$, respectively.

The increasing $\Gamma_{\text{LO}}^{\text{doped}} - \Gamma_{\text{LO}}$ with T in the regime of delocalized electrons can be attributed to plasmon damping by electron collisions.² The collision rates become larger as more electrons are thermally promoted to the conduction band, thus producing a larger phenomenological plasmon damping with T . This damping smears the plasma response of the electron gas which in turn broadens the coupled phonon-plasma mode. When the electrons are localized, the low- T broadening is the imaginary part of the phonon self-energy due to the interaction with the continuum. The discrete-continuum interaction theory predicts for the broadening,^{1,2}

$$\Gamma_{\text{LO}}^{\text{doped}} - \Gamma_{\text{LO}} = \pi V^2 \rho(E). \quad (4)$$

We have found an empirical correlation between the

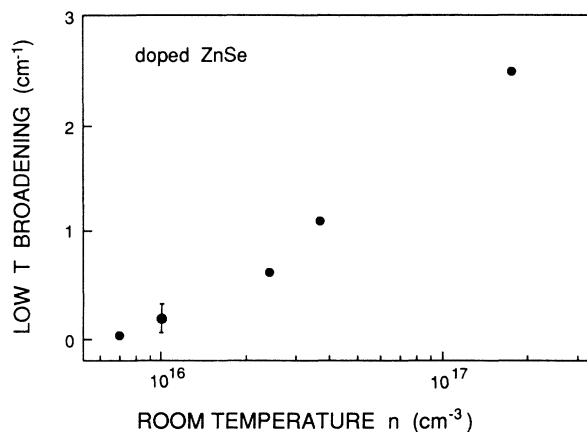


FIG. 6. Low-temperature (13 K) broadening of the Raman lines of doped ZnSe layers plotted against the free-electron density at room temperature. The Raman data corresponds to the 488.0-nm layer excitation and have been corrected for instrumental resolution. An empirical correlation is found.

broadening $\Gamma_{\text{LO}}^{\text{doped}} - \Gamma_{\text{LO}}$ at 13 K and the electron concentration at room temperature n (300 K). The plot in Fig. 6 establishes an almost linear relationship in the semilogarithmic graph. If we assume that V does not change with doping and consider that in lightly compensated samples $n(300) \approx N_D$, the plot in Fig. 6 will indicate that $\rho(E)$ is not linearly proportional to N_D . The departure from a linear dependence particularly at the highest N_D

can be taken as additional indication of wave-function overlap.¹

V. CONCLUSIONS

The aim of this work has been to provide some basic experimental information on intrinsic properties of phonons and electrons in a typical wide-band-gap semiconductor. We focused on the general characteristics of the coupling between electrons and longitudinal-optical phonons in n -type ZnSe layers, which were doped below the Mott criterion for the metal-insulator transition. We showed that phonon-plasmon coupling dominates when free electrons populate delocalized states in the conduction band. A discrete-continuum interaction prevails when electrons are localized in donor states and gives rise to asymmetrical Fano line shapes in the phonon spectra. In addition, we have obtained data and found empirical correlations for future characterization of these materials. We have determined carrier concentrations, established a relationship between phonon linewidths at low temperature and carrier concentration, and observed Raman scattering from donors. These results open possibilities for further investigations of fundamental properties of wide-band-gap semiconductors. Among them are the evolution of the electron-phonon interaction as the insulator-metal transition is approached and the electron-electron scattering in the electron gas. Also, comparisons of activation energies for transport processes and the spectroscopic determinations of bound electronic transitions should help in the understanding of the formation of impurity bands.

¹M. V. Klein, in *Light Scattering in Solids*, edited by M. Cardona (Springer, Heidelberg, 1975), p. 147 and references therein.

²G. Abstreiter, M. Cardona, and A. Pinczuk, in *Light Scattering in Solids*, edited by M. Cardona and G. Guntherodt (Springer, Heidelberg, 1984), p. 5 and references therein.

³See, for example, Proceedings of the Fourth International Conference on II-VI Compounds [J. Crystal Growth **101** (1990)].

⁴P. J. Dean, D. C. Herbert, C. J. Werkhoven, B. J. Fitzpatrick, and R. N. Bhargava, Phys. Rev. B **23**, 4888 (1981).

⁵H. E. Ruda, J. Appl. Phys. **59**, 1220 (1986).

⁶T. Marshall and J. Gaines, Appl. Phys. Lett. **56**, 2669 (1990).

⁷A. Y. Cho, in *The Technology and Physics of Molecular Beam Epitaxy*, edited by E. H. C. Parker (Plenum, London, 1985),

p. 1.

⁸H. Hartmann, R. Mach, and B. Selle, in *Current Topics in Materials Science*, edited by E. Kaldis (North-Holland, Amsterdam, 1982), Vol. 9, p. 1 and references therein.

⁹J. L. La Combe and J. C. Irwin, Solid State Commun. **8**, 1427 (1970).

¹⁰M. Balkanski, R. F. Wallis, and E. Haro, Phys. Rev. B **28**, 1928 (1983).

¹¹J. Menendez and M. Cardona, Phys. Rev. B **29**, 2051 (1984).

¹²C. H. Henry and J. J. Hopfield, Phys. Rev. B **6**, 2233 (1972).

¹³P. J. Dean, H. Venghaus, J. C. Pfister, B. Schaub, and J. Marine, J. Lumin. **16**, 363 (1978).

¹⁴K. Shahzad, B. Kahn, D. J. Olego, and D. Cammack (unpublished).